JOURNAL OF AIRCRAFT
Vol. 44, No. 1, January–February 2007

Aerodynamic Modeling of Morphing Wings Using an Extended Lifting-Line Analysis

Adam M. Wickenheiser* and Ephrahim Garcia†
Cornell University, Ithaca, New York 14853

DOI: 10.2514/1.18323

This paper presents an extension of Weissinger's method and its use in analyzing morphing wings. This method is shown to be ideal for preliminary analyses of these wings due to its speed and adaptability to many disparate wing geometries. It extends Prandtl's lifting-line theory to planform wings of arbitrary curvature and chord distribution and nonideal airfoil cross sections. The problem formulation described herein leads to an integrodifferential equation for the unknown circulation distribution. It is solved using Gaussian quadrature and a sine-series representation of this distribution. In this paper, this technique is used to analyze the aerodynamics of a morphable gull-like wing. Specifically, this wing's ability to manipulate lift-to-drag efficiency and center of pressure location is discussed.

Nomenclature

a = wing curvature parameter
b = wing span
C_l = section lift coefficient
C_d = section drag coefficient
C_L = wing lift force coefficient
C_D = wing drag force coefficient
C_Y = wing side force coefficient
$C_{\mathcal{L}}$ = wing roll moment coefficient
$C_{\mathcal{M}}$ = wing pitch moment coefficient
$C_{\mathcal{N}}$ = wing yaw moment coefficient
C_{l_α} = section lift curve slope
c = local chord length
$\hat{c}$ = local nondimensional chord length
$\bar{c}$ = mean aerodynamic chord
$\hat{\bar{c}}$ = nondimensional mean aerodynamic chord
G = nondimensional circulation
L = wing lift force
l = section lift force/length
M = number of points used in trapezoidal approximation
m = number of points used in sine-series expansion of circulation function
Q = dynamic pressure
$\boldsymbol{r}$ = displacement vector
S = wing planform area
$\hat{S}$ = nondimensional wing planform area
U_∞ = free-stream velocity magnitude
$\boldsymbol{v}$ = wind velocity vector
w = downwash velocity
x_{cg} = position of the wing center of gravity
x_{cp} = position of the wing center of pressure
$x_{c/4}$ = position of the airfoil quarter-chord point
y_0 = wing semispan, y coordinate of wingtip
α = wind incidence angle/angle of attack
α_{0L} = angle of attack for zero lift
Γ = circulation magnitude
Γ = vorticity vector
ε = downwash angle at wing 1/4-chord line
η = nondimensional spanwise coordinate
Λ = wing aspect ratio
ξ = nondimensional chordwise coordinate
σ = planar density
$\mathcal{L}$ = wing roll moment
$\mathcal{M}$ = wing pitch moment
$\mathcal{N}$ = wing yaw moment

Received 21 June 2005; revision received 20 March 2006; accepted for publication 20 March 2006.

*Graduate Student, Sibley School of Mechanical & Aerospace Engineering, 226 Upson Hall. Student Member AIAA.
†Associate Professor, Sibley School of Mechanical & Aerospace Engineering, 224 Upson Hall. Member AIAA.

Introduction

THROUGHOUT the history of aviation, very little of man's inspiration for flight has manifested itself in aircraft designs. Indeed, man-made flight bears little resemblance to avian morphologies, which are backed by millions of years of evolution. Birds morph their wings and tail in complex, fluid ways, in contrast to the limited range of motion of an aircraft's control surfaces. Most aircraft deploy flaps and slats during takeoff and landing in order to increase lift at slower speeds. This is an example of a configuration change that occurs continuously during avian flight. A bird's morphology allows it to constantly change its wing and tail shapes to suit flight at a wide range of speeds.

Recently, research and development have begun on a new concept that challenges current designs: morphing aircraft [1]. A morphing aircraft is an aircraft capable of controlled, gross shape changes in-flight, with the purpose of increasing efficiency, versatility, and/or mission performance. Whereas traditional aircraft are designed as compromises of various performance needs, a single morphing aircraft can excel at numerous tasks [2,3]. The same airframe can morph from a highly efficient glider to a fast, high maneuverability vehicle. Whereas a traditional wing is designed for high efficiency over a small range of flight conditions, a morphing wing can adapt to grossly different altitudes and flight speeds. Morphing technologies enable new flight capabilities, such as perching, urban navigation, and indoor flight. These capabilities have heretofore been unrealizable due to technological limitations. Modern development of smart structures, adaptive materials, and distributed and adaptive control theory has opened the door to a host of new aircraft designs and flight capabilities [4].

These new capabilities are realized by the careful manipulation of aerodynamic forces and moments. For example, a long endurance aircraft benefits from a high lift-to-drag ratio, whereas a highly maneuverable aircraft needs high lift and low (or negative) stability margins. Highly efficient cruise can be accomplished by morphing the wing cross sections to maintain high lift-to-drag ratios at various flight speeds and altitudes. New capabilities, such as perching, can be achieved by controlling the degree of separated flow over the

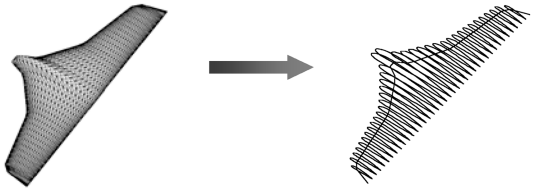

Fig. 1 Lifting-line theory effectively decouples the 3-D panel problem into a series of 2-D airfoils.

aircraft's lifting surfaces [5]. Many of these capabilities require levels of actuation far exceeding the bounds of conventional aircraft control surfaces.

Unlike most traditional aircraft, morphing aircraft concepts require an aerodynamic analysis for both varying flight conditions and grossly varying geometric configurations. This requirement demands a preliminary analysis methodology that is fast, accurate, and reconfigurable, without having to rebuild the mesh of the aircraft or flow field, for example. Consequently, a lifting-line approach is chosen over a computational fluid dynamics (CFD) approach as the aerodynamic modeling method. This method effectively breaks the 3-D wing into a series of 2-D airfoils joined by their quarter-chord curve, as depicted in Fig. 1. The analytic nature of this method allows the wing geometries to be programmed as functions into generic software environments such as Matlab or *C*. Consequently, changing geometry parameters, such as the wing curvature parameter presented below, may be placed in a software loop in order to automatically generate many wing geometry variations.

Weissinger's method for straight, swept wings is the basis of the present lifting-line theory [6]. His method relates the downwash air velocity at any given span station on the wing to the sum of the downwash contributions of the vortex line attached to the quarter-chord line of the wing and the semi-infinite vortex sheet trailing behind it. This method does not consider the geometry of the wing cross sections or the nonplanarity of the wake. An effort is made, as explained below, to account for the former by introducing real airfoil data for each of the span stations. Although full 3-D analysis tools such as panel methods and CFD software do not require a separate database of airfoil data in this event, computationally it is more efficient to have these data tabulated beforehand. The method presented below only has to reference these data instead of needing to recompute them in its algorithm. This method has been extended to curved wings of a specific (polynomial) form by Prössdorf and Tordella [7] for stationary wings and by Chiocchia, et al. [8] for wings in oscillatory motion.

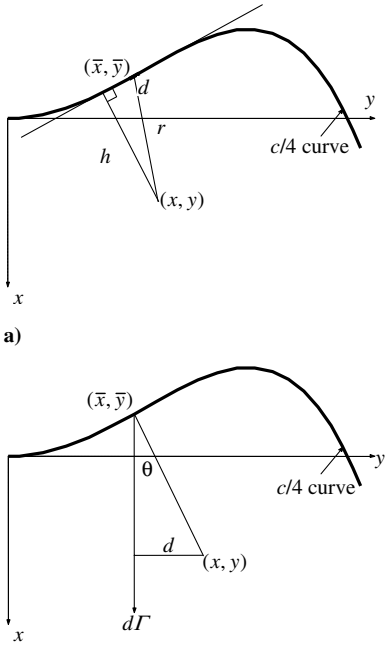

Fig. 2 a) Schematic of the downwash contribution by a segment ds of the lifting vortex. b) Schematic of the downwash contribution by a vortex filament $d\Gamma$ of the tailing vortex system.

The problem formulation leads to an integrodifferential equation as shown in the next section. This equation is solved assuming a sine-series representation of the circulation, which conforms to the boundary conditions of no circulation at the wingtips. Gaussian quadrature and the trapezoidal rule are then used to compute the integrals. This technique results in a relatively high $1/M^2$ error, where M is the number of function evaluations; however, this number may be increased independently from the number of span stations m used in the aerodynamic calculations, as shown below. Prössdorf shows that error in the calculated circulation distribution decreases exponentially with m, assuming that the quarter-chord curve can be bounded by a polynomial [7].

This analysis is shown to be effective in computing the lift and drag distributions over a variety of wing geometries. Although this method assumes no separation effects, it is valid in the Reynolds number regime of medium-scale UAVs and larger aircraft at moderate angles of attack, where viscous effects are minimal. This method's speed and reconfigurability make it ideal for the preliminary analysis of morphing wings with a large number of varying geometrical parameters. This method is also useful in the construction of an aerodynamic lookup table for use in a aircraft simulation, for example.

Problem Formulation

A model of the wing geometry and the flow field is developed in order to formulate the circulation distribution along the span. The circulation is found by examining the downwash velocity distribution in the wake of the lifting surface. First, a Cartesian coordinate system is established such that the positive x direction points downstream, parallel to the free-stream velocity U_∞, and the positive y direction points towards the right wingtip. (Thus, by the right-hand rule, the positive z direction points outward from the page.) The quarter chord of the wing is represented by a continuous, piecewise differentiable function that extends from $y = -y_0$ to $y = y_0$, not necessarily symmetric about the x axis but contained entirely in the xy plane. The chord and twist distributions are given as piecewise continuous functions of the spanwise coordinate. The model of the flow field consists of a bound or lifting vortex at the quarter-chord curve of the wing and a trailing vortex sheet that extends to infinity downstream. The downwash at each point in the flow field is therefore the sum of the velocities induced by the lifting vortex and the distributed vortex sheet. These two contributions are shown in Fig. 2, where the geometry is defined in a similar manner to Prössdorf [7] and DeYoung [9]. Because the flow field is modeled as a superposition of potential flows, this method only applies when viscous effects are not significant.

The contributions of the lifting and trailing vortices to the downwash velocity w can be calculated by the Biot-Savart Law:

$$\boldsymbol{v} = \frac{1}{4\pi} \int \frac{\Gamma \times \boldsymbol{r}}{|\boldsymbol{r}|^3} \, \mathrm{d}s \tag{1}$$

which gives the fluid velocity at any point displaced from a vortex element of strength Γ. Using this law, the downwash caused by segment ds of the lifting vortex is given by

$$\mathrm{d}w(x, y) = \frac{\Gamma h \, \mathrm{d}s}{4\pi r^3} \tag{2}$$

where the geometry is defined in Fig. 2a. In terms of the points (x, y) in the plane of the wing and $(\bar{x}, \bar{y})$ along the quarter-chord curve, Eq. (2) becomes

$$\mathrm{d}w(x, y) = \Gamma(\bar{y}) \frac{[x - \bar{x}(\bar{y}) + \bar{x}'(\bar{y})(\bar{y} - y)] \, \mathrm{d}\bar{y}}{4\pi\{[x - \bar{x}(\bar{y})]^2 + (y - \bar{y})^2\}^{3/2}} \tag{3}$$

where

$$\bar{x}'(\bar{y}) = \left.\frac{d\bar{x}(y)}{dy}\right|_{y=\bar{y}}$$

The downwash caused by an infinitesimal vortex filament $d\Gamma$ in the trailing vortex sheet is given by

$$dw(x, y) = \frac{d\Gamma}{4\pi d}(\cos\theta + 1) \tag{4}$$

where the geometry is defined in Fig. 2b. In terms of the points (x, y) and $(\bar{x}, \bar{y})$, Equation (4) becomes

$$dw(x, y) = \frac{\Gamma'(\bar{y})}{4\pi(y-\bar{y})}\left(\frac{x-\bar{x}(\bar{y})}{\sqrt{[x-\bar{x}(\bar{y})]^2 + (y-\bar{y})^2}} + 1\right) d\bar{y} \tag{5}$$

where

$$\Gamma'(\bar{y}) = \left.\frac{d\Gamma(y)}{dy}\right|_{y=\bar{y}}$$

Summing Eqs. (3) and (5) and integrating from $-y_0$ to y_0 gives the total downwash at the point (x, y) in the flow field:

$$\begin{aligned} w(x, y) = {} & \frac{1}{4\pi}\int_{-y_0}^{y_0} \frac{\Gamma'(\bar{y})}{y-\bar{y}}\, d\bar{y} \\ & + \frac{1}{4\pi}\int_{-y_0}^{y_0} \frac{\Gamma'(\bar{y})}{y-\bar{y}} \frac{x-\bar{x}(\bar{y})}{\sqrt{[x-\bar{x}(\bar{y})]^2 + (y-\bar{y})^2}}\, d\bar{y} \\ & + \frac{1}{4\pi}\int_{-y_0}^{y_0} \Gamma(\bar{y}) \frac{x-\bar{x}(\bar{y}) + \bar{x}'(\bar{y})(\bar{y}-y)}{\{[x-\bar{x}(\bar{y})]^2 + (y-\bar{y})^2\}^{3/2}}\, d\bar{y} \end{aligned} \tag{6}$$

The first two integrals in Eq. (6) have singularities at $\bar{y} = y$; however, only the second integral diverges near the singularity. (The singularity in the first integral will be addressed below.) To remove this discontinuity, the first term is added to and subtracted from Eq. (6), as recommended by DeYoung [9], resulting in

$$\begin{aligned} w(x, y) = {} & \frac{1}{2\pi}\int_{-y_0}^{y_0} \frac{\Gamma'(\bar{y})}{y-\bar{y}}\, d\bar{y} \\ & + \frac{1}{4\pi}\int_{-y_0}^{y_0} \frac{\Gamma'(\bar{y})}{y-\bar{y}}\left[\frac{x-\bar{x}(\bar{y})}{\sqrt{[x-\bar{x}(\bar{y})]^2 + (y-\bar{y})^2}} - 1\right] d\bar{y} \\ & + \frac{1}{4\pi}\int_{-y_0}^{y_0} \Gamma(\bar{y}) \frac{x-\bar{x}(\bar{y}) + \bar{x}'(\bar{y})(\bar{y}-y)}{\{[x-\bar{x}(\bar{y})]^2 + (y-\bar{y})^2\}^{3/2}}\, d\bar{y} \end{aligned} \tag{7}$$

which is referred to as the dimensional form of the modified Weissinger's method. According to the Pistolesi-Weissinger condition [6], the overall wind velocity should be tangent to the plane of the wing at the wing's $\frac{3}{4}$-chord line. In other words, along this line the downwash angle is equal to the local airfoil's angle of attack, which is the sum of the wing's geometrical twist and its overall angle of attack. Thus, the downwash velocity w in Eq. (7) should be evaluated at

$$x = \bar{x}(y) + \frac{c(y)}{2} \tag{8}$$

which is half a chord length behind the quarter-chord line. With this substitution, Eq. (7) becomes

$$\begin{aligned} w(y) = {} & \frac{1}{2\pi}\int_{-y_0}^{y_0} \frac{\Gamma'(\bar{y})}{y-\bar{y}} d\bar{y} \\ & + \frac{1}{4\pi}\int_{-y_0}^{y_0} \frac{\Gamma'(\bar{y})}{y-\bar{y}}\left[\frac{\bar{x}(y) - \bar{x}(\bar{y}) + c(y)/2}{\sqrt{(\bar{x}(y) - \bar{x}(\bar{y}) + c(y)/2)^2 + (y-\bar{y})^2}} - 1\right] d\bar{y} \\ & + \frac{1}{4\pi}\int_{-y_0}^{y_0} \Gamma(\bar{y}) \frac{\bar{x}(y) - \bar{x}(\bar{y}) + c(y)/2 + \bar{x}'(\bar{y})(\bar{y}-y)}{[(\bar{x}(y) - \bar{x}(\bar{y}) + c(y)/2)^2 + (y-\bar{y})^2]^{3/2}} d\bar{y} \end{aligned} \tag{9}$$

where the downwash is now only a function of the spanwise coordinate. If the geometry for a straight, swept wing is substituted into Eq. (9), then the lifting-line formula derived by Weissinger [6] and DeYoung [9] can be recovered.

Solution Procedure

Equation (9) gives the downwash caused by the lifting vortex and the trailing vortex sheet at the point y along the $\frac{3}{4}$-chord line; this downwash should be equal to the upwash felt by the wing due to its local incidence to the flow. Therefore, the only unknown quantity in Eq. (9) is the circulation distribution $\Gamma(y)$. Although $\Gamma(y)$ has no explicit solution, it can be approximated to an arbitrary accuracy by a sine series, as first shown by Multhopp [10]. A transformation to trigonometric coordinates will then allow the exact integration of the first term in Eq. (9) and a simplification of the other two terms. The trapezoidal method is then used to integrate the second and third terms. As will be shown, the number of terms used in this integration can be made independent of the number of terms used in the sine-series representation of $\Gamma(y)$.

It is now convenient to convert Eq. (9) to nondimensional form by introducing the following dimensionless variables:

$$\eta = \frac{y}{y_0}, \qquad \bar{\eta} = \frac{\bar{y}}{y_0}, \qquad G = \frac{\Gamma}{y_0 U_\infty}, \qquad \bar{\xi} = \frac{\bar{x}}{c}, \qquad \alpha = \frac{w}{U_\infty} \tag{10}$$

Here, it is assumed that all downwash angles are small. In dimensionless form, Eq. (9) can now be written as

$$\begin{aligned} \alpha(\eta) = {} & \frac{1}{2\pi}\int_{-1}^{1} \frac{G'(\bar{\eta})}{\eta-\bar{\eta}}\, d\bar{\eta} + \frac{1}{4\pi}\int_{-1}^{1} \frac{G'(\bar{\eta})}{\eta-\bar{\eta}}\left[\frac{\bar{\xi}(\eta) - \bar{\xi}(\bar{\eta}) + \frac{1}{2}}{\sqrt{[\bar{\xi}(\eta) - \bar{\xi}(\bar{\eta}) + 1/2]^2 + [y_0/c(\eta)]^2(\eta-\bar{\eta})^2}} - 1\right] d\bar{\eta} \\ & + \frac{1}{4\pi}\left(\frac{y_0}{c(\eta)}\right)^2 \int_{-1}^{1} G(\bar{\eta}) \frac{\bar{\xi}(\eta) - \bar{\xi}(\bar{\eta}) + \frac{1}{2} + \bar{\xi}'(\bar{\eta})(\bar{\eta}-\eta)}{\left\{\left[\bar{\xi}(\eta) - \bar{\xi}(\bar{\eta}) + \frac{1}{2}\right]^2 + [y_0/c(\eta)]^2(\eta-\bar{\eta})^2\right\}^{3/2}} d\bar{\eta} \end{aligned} \tag{11}$$

To simplify the integrals in Eq. (11) and cast $G(\bar{\eta})$ as a sine series, the spanwise coordinates are transformed into angles by the following definitions:

$$\phi_v \equiv \cos^{-1}(\eta) \quad \text{and} \quad \phi \equiv \cos^{-1}(\bar{\eta}) \tag{12}$$

For simplicity, let

$$P(\eta, \bar{\eta}) \equiv \frac{1}{\eta-\bar{\eta}}\left[\frac{\bar{\xi}(\eta) - \bar{\xi}(\bar{\eta}) + \frac{1}{2}}{\sqrt{[\bar{\xi}(\eta) - \bar{\xi}(\bar{\eta}) + \frac{1}{2}]^2 + [y_0/c(\eta)]^2(\eta-\bar{\eta})^2}} - 1\right], \qquad R(\eta, \bar{\eta}) \equiv \frac{\bar{\xi}(\eta) - \bar{\xi}(\bar{\eta}) + \frac{1}{2} + \bar{\xi}'(\bar{\eta})(\bar{\eta}-\eta)}{\{[\bar{\xi}(\eta) - \bar{\xi}(\bar{\eta}) + \frac{1}{2}]^2 + [y_0/c(\eta)]^2(\eta-\bar{\eta})^2\}^{3/2}} \tag{13}$$

After these substitutions, Eq. (11) becomes

$$\alpha(\phi_v) = \frac{1}{2\pi}\int_0^\pi \frac{G'(\phi)}{\cos\phi - \cos\phi_v}\,\mathrm{d}\phi - \frac{1}{4\pi}\int_0^\pi P(\phi_v,\phi)G'(\phi)\,\mathrm{d}\phi + \frac{1}{4\pi}\left(\frac{y_0}{c(\phi_v)}\right)^2\int_0^\pi R(\phi_v,\phi)G(\phi)\sin\phi\,\mathrm{d}\phi \tag{14}$$

To solve Eq. (14) for the unknown function $G(\phi)$, it is assumed that $G(\phi)$ can be represented as a sine series of m terms. (Note that this representation meets the boundary conditions of no circulation at the wingtips, that is $G(0) = G(\pi) = 0$.) Let

$$G(\phi) = \sum_{k=1}^{m} a_k \sin(k\phi), \quad \text{where } a_k = \frac{2}{\pi}\int_0^\pi G(\phi)\sin(k\phi)\mathrm{d}\phi \tag{15}$$

Multhopp's formula [10], based on Gaussian quadrature, is used to evaluate the integral in Eq. (15). This method will exactly integrate a sequence of orthogonal functions such as the sine-series representation of $G(\phi)$ if m points are chosen for the quadrature. These points must be located at the roots of the next function in the sequence, $\sin[(m+1)\pi]$. Applying this quadrature to Eq. (15) yields

$$a_k = \frac{2}{m+1}\sum_{n=1}^{m} G(\phi_n)\sin(k\phi_n), \quad \text{where } \phi_n = \frac{n\pi}{m+1} \tag{16}$$

where the ϕ_n are the roots of the next function in the sine series. Therefore,

$$\begin{aligned} G(\phi) &= \frac{2}{m+1}\sum_{n=1}^{m} G(\phi_n)\sum_{k=1}^{m}\sin(k\phi_n)\sin(k\phi) \\ G'(\phi) &= \frac{2}{m+1}\sum_{n=1}^{m} G(\phi_n)\sum_{k=1}^{m} k\sin(k\phi_n)\cos(k\phi) \end{aligned} \tag{17}$$

With the definitions

$$\begin{aligned} f_n(\phi) &\equiv \frac{2}{m+1}\sum_{k=1}^{m}\sin(k\phi_n)\sin(k\phi) \\ h_n(\phi) &\equiv \frac{2}{m+1}\sum_{k=1}^{m} k\sin(k\phi_n)\cos(k\phi) \qquad G_n \equiv G(\phi_n) \end{aligned} \tag{18}$$

Equation (17) can be written as

$$G(\phi) = \sum_{n=1}^{m} G_n f_n(\phi) \quad \text{and} \quad G'(\phi) = \sum_{n=1}^{m} G_n h_n(\phi) \tag{19}$$

Substituting Eqs. (18) and (19) into Eq. (14) gives

$$\alpha(\phi_v) = \frac{1}{\pi(m+1)}\sum_{n=1}^{m} G_n \sum_{k=1}^{m} k\sin(k\phi_n)\int_0^\pi \frac{\cos(k\phi)}{\cos\phi - \cos\phi_v}\,\mathrm{d}\phi - \frac{1}{4\pi}\sum_{n=1}^{m} G_n\int_0^\pi P(\phi_v,\phi)h_n(\phi)\,\mathrm{d}\phi + \frac{1}{4\pi}\left(\frac{y_0}{c(\phi_v)}\right)^2\sum_{n=1}^{m} G_n\int_0^\pi R(\phi_v,\phi)f_n(\phi)\sin\phi\,\mathrm{d}\phi \tag{20}$$

Although the first integral has a singularity at $\phi = \phi_v$, the integral is finite and given by the formula

$$\int_0^\pi \frac{\cos(k\phi)}{\cos\phi - \cos\phi_v}\,\mathrm{d}\phi = \frac{\pi\sin(k\phi_v)}{\sin\phi_v} \tag{21}$$

derived by Glauert [11]. The trapezoidal method is used to evaluate the second and third integrals in Eq. (20). This formula is given by

$$\int_0^\pi F(\phi)\,\mathrm{d}\phi \approx \frac{\pi}{M+1}\left[\frac{F(0)+F(\pi)}{2} + \sum_{\mu=1}^{M} F(\phi_\mu)\right] \tag{22}$$

where

$$\phi_\mu = \frac{\mu\pi}{M+1}$$

for a general function $F(\phi)$. The integer M dictates how many function evaluations are used to compute the integral and is independent of m, the number of terms in the sine-series representation of $G(\phi)$. Using Eqs. (21) and (22) to evaluate the integrals in Eq. (20) gives

$$\begin{aligned} \alpha(\phi_v) = {} & \frac{1}{m+1}\sum_{n=1}^{m} G_n \sum_{k=1}^{m}\frac{k\sin(k\phi_n)\sin(k\phi_v)}{\sin\varphi_v} \\ & - \frac{1}{4(M+1)}\sum_{n=1}^{m} G_n\left[\frac{P(\phi_v,0)h_n(0) + P(\phi_v,\pi)h_n(\pi)}{2} + \sum_{\mu=1}^{M} P(\phi_v,\phi_\mu)h_n(\phi_\mu)\right] \\ & + \frac{1}{4(M+1)}\left(\frac{y_0}{c(\phi_v)}\right)^2\sum_{n=1}^{m} G_n\sum_{\mu=1}^{M} R(\phi_v,\phi_\mu)f_n(\phi_\mu)\sin\phi_\mu \end{aligned} \tag{23}$$

The sum in the first term of Eq. (23) has an explicit formula, given by

$$\frac{1}{m+1}\sum_{k=1}^{m}\frac{k\sin(k\phi_n)\sin(k\phi_v)}{\sin\phi_v} = \begin{cases} \frac{m+1}{4\sin\phi_v}, & n = v \\ \frac{-\sin\phi_n}{(\cos\phi_n - \cos\phi_v)^2}, & n \neq v \end{cases} \tag{24}$$

Equation (23) relates the airfoil angle of attack at ϕ_v to a linear combination of circulation function evaluations G_n. Since $\alpha(\phi)$ is a known function, it can be evaluated at m distinct points to create a system of equations for G_n. Constructing the matrix

$$\begin{aligned} \mathbf{A} = {} & \frac{1}{m+1}\sum_{k=1}^{m}\frac{k\sin(k\phi_n)\sin(k\phi_v)}{\sin\phi_v} \\ & - \frac{1}{4(M+1)}\left[\frac{P(\phi_v,0)h_n(0) + P(\phi_v,\pi)h_n(\pi)}{2} + \sum_{\mu=1}^{M} P(\phi_v,\phi_\mu)h_n(\phi_\mu)\right] \\ & + \frac{1}{4(M+1)}\left(\frac{y_0}{c(\phi_v)}\right)^2\sum_{\mu=1}^{M} R(\phi_v,\phi_\mu)f_n(\phi_\mu)\sin\phi_\mu \end{aligned} \tag{25}$$

where the vnth component is evaluated at ϕ_v and ϕ_n, Eq. (23) becomes

$$\boldsymbol{\alpha} = \mathbf{A}\boldsymbol{G}, \quad \text{where } \boldsymbol{\alpha} = \begin{bmatrix} \alpha(\phi_1) \\ \vdots \\ \alpha(\phi_m) \end{bmatrix} \quad \text{and} \quad \boldsymbol{G} = \begin{bmatrix} G_1 \\ \vdots \\ G_m \end{bmatrix} \tag{26}$$

This is a system of m equations for the unknowns G_n. The vector $\boldsymbol{\alpha}$ comprises the local angle of attack values at $\phi_1, \ldots, \phi_m$, and $\boldsymbol{G}$ is a vector of unknowns. The G_n can be computed by inverting $\mathbf{A}$, and the circulation distribution can be reconstructed using Eq. (19).

So far, this analysis has assumed that the airfoil cross sections of the wing are ideal; that is, they have a lift curve slope of 2π and generate no lift at a zero-degree angle of attack. It is desired to incorporate real airfoil data into this lifting-line analysis in order to predict better the lift on real aircraft wings. This incorporation will also help evaluate the effects of airfoil morphing on the entire wing's aerodynamic properties. These data may be obtained from experiment or computation; however, as stated previously, they are only referenced by this algorithm and not recomputed. To assimilate nonideal airfoils, DeYoung suggests the method of distorting the chord length distribution along the wing such that the dimensional circulation about every span station matches the dimensional circulation of an ideal airfoil with the original chord length [9].

Alternatively, this can be accomplished by offsetting the left-hand side of Eq. (23) by the true angle of attack for zero lift of that section and scaling it by the ratio of its lift curve slope to that of an ideal airfoil. Consequently, the left-hand side becomes

$$\frac{c_{l_\alpha}(\phi_v)}{2\pi}[\alpha(\phi_v) - \alpha_{0L}(\phi_v)] = \cdots \tag{27}$$

The downwash angle at each wing station can now be computed. By Munk's analysis [12], the downwash angle is given by half the downwash angle an infinite distance downstream. To calculate this, take half the limit of Eq. (7) as x goes to infinity:

$$\tfrac{1}{2}\lim_{x\to\infty} w(x, y) = \frac{1}{4\pi}\int_{-y_0}^{y_0} \frac{\Gamma'(\bar{y})}{y - \bar{y}}\,\mathrm{d}\bar{y} \tag{28}$$

By converting Eq. (28) to nondimensional form and casting it terms of the sine-series coefficients, the downwash angle ε at station ϕ_v is given by

$$\varepsilon(\phi_v) = \frac{1}{2(m+1)}\sum_{n=1}^{m} G_n \sum_{k=1}^{m} \frac{k\sin(k\phi_n)\sin(k\phi_v)}{\sin\phi_v} \tag{29}$$

which is one half the first term in Eq. (23). With the downwash angle given by Eq. (29), the overall wind incidence angle (wing angle of attack + wing twist + downwash angle) can be computed at each station. Although this angle is computed using potential theory, it can be used to acquire a good approximation of section lift and drag forces if real airfoil data are available. The overall wind incidence angle is used in lieu of the angle of attack in determining section lift (C_l) and drag (C_d) coefficients. These coefficients are then rotated back into the xz-coordinate system by the angle ε as given by

$$^{xz}\begin{bmatrix} C_l \\ C_d \end{bmatrix} = \begin{bmatrix} \cos\varepsilon & -\sin\varepsilon \\ \sin\varepsilon & \cos\varepsilon \end{bmatrix}^{\text{wind}}\begin{bmatrix} C_l \\ C_d \end{bmatrix} \tag{30}$$

where superscript xz indicates the xz-coordinate system and superscript "wind" indicates the local wind coordinate system.

Using the standard definitions of lift coefficient (C_L) and section lift coefficient (C_l),

$$C_L = \frac{L}{QS} \quad \text{and} \quad C_l = \frac{l}{Qc} \tag{31}$$

a straightforward integration of these coefficients over the entire wing gives the overall lift and pitching moments of the wing. Starting with the relation between lift and section lift

$$L = \int_{-b/2}^{b/2} l\,\mathrm{d}y \tag{32}$$

the lift coefficient can then be calculated by

$$C_L = \frac{1}{\hat{S}}\int_{-1}^{1} C_l\hat{c}\,\mathrm{d}\eta \tag{33}$$

Similarly, the drag coefficient is given by

$$C_D = \frac{1}{\hat{S}}\int_{-1}^{1} C_d\hat{c}\,\mathrm{d}\eta \tag{34}$$

In this problem formulation, side forces are considered negligible; therefore,

$$C_Y = 0 \tag{35}$$

The moment coefficients are also calculated in a straightforward manner. Starting from the definitions of pitch, roll, and yaw moment coefficients,

$$C_{\mathcal{M}} = \frac{\mathcal{M}}{QS\bar{c}}, \qquad C_{\mathcal{L}} = \frac{\mathcal{L}}{QSb}, \quad \text{and} \quad C_{\mathcal{N}} = \frac{\mathcal{N}}{QSb} \tag{36}$$

respectively, the moment coefficients can be calculated using the section lift and drag coefficients as follows:

$$C_{\mathcal{M}} = \frac{1}{\hat{S}\,\hat{\bar{c}}}\int_{-1}^{1} C_l\hat{c}\hat{\xi}\,\mathrm{d}\eta, \qquad C_{\mathcal{L}} = \frac{1}{2\hat{S}}\int_{-1}^{1} C_l\hat{c}\eta\,\mathrm{d}\eta$$
$$C_{\mathcal{N}} = \frac{1}{2\hat{S}}\int_{-1}^{1} C_d\hat{c}\eta\,\mathrm{d}\eta \tag{37}$$

Two other important parameters in wing design are the centers of pressure and gravity. The displacement between these two points is very important in determining the stability and dynamic response of the wing in an unsteady flight condition and in determining the dynamics of the overall aircraft system. In the context of the prescribed geometry, the center of pressure relative to the origin is calculated as follows:

$$Lx_{\text{cp}} = \mathcal{M} \qquad x_{\text{cp}} = \frac{1}{L}\int_{-b/2}^{b/2} lx_{c/4}\,\mathrm{d}y \tag{38}$$

Similarly, the center of gravity is equal to

$$x_{cg} = \frac{\int_{-b/2}^{b/2}\sigma x\,\mathrm{d}y}{\int_{-b/2}^{b/2}\sigma\,\mathrm{d}y} = \frac{\int_{-b/2}^{b/2} c^2 x\,\mathrm{d}y}{\int_{-b/2}^{b/2} c^2\,\mathrm{d}y} \tag{39}$$

Here, it is assumed that the density of the wing is constant, which leads to a square variation of mass with respect to chord length.

Results

Using the methods described in the previous section, circulation, downwash, and force distributions are calculated for several wing shapes, as well as overall wing parameters such lift, drag, and center of pressure location. This method's relatively loose requirements for wing geometry enable some nontraditional wings to be analyzed. Along the vein of bioinspiration, a gull wing shape is chosen as the basis of this analysis. This wing features forward- and aft-swept wing sections that can be utilized for c.g. and c.p. adjustments, as discussed below. The wing is described by the quarter-chord curve

$$x(y) = a\left[\left(\frac{y}{ky_0}\right)^4 - \left(\frac{y}{ky_0}\right)^2\right] \tag{40}$$

and shown in Fig. 3 for various values of curvature parameter a. (A value of $k = \sqrt{3/7}$ is chosen in order to maintain a constant c.g. location for all values of a, assuming a constant density wing as described previously.) For this analysis, every wing shape is constructed using an elliptical chord distribution such that a direct comparison of these wings with the canonical straight, elliptical wing can be made. Also, the same root chord length is used throughout in order to maintain a constant aspect ratio of 10. Although this analysis may be used for any angle of attack within the range of validity of

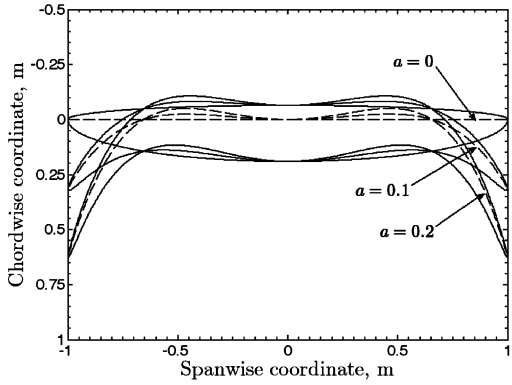

Fig. 3 Gull wings of constant span with curvature parameter $a = 0$, 0.1, 0.2.

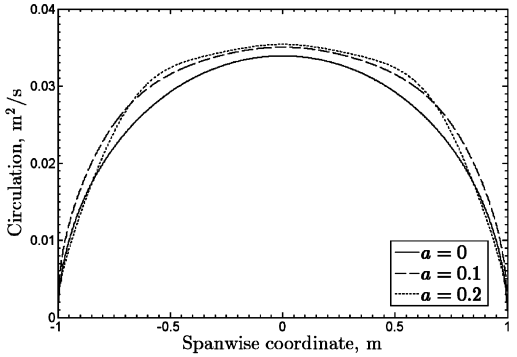

Fig. 4 Circulation distribution of several gull wings, $\Lambda = 10$, $\alpha = 3$ deg.

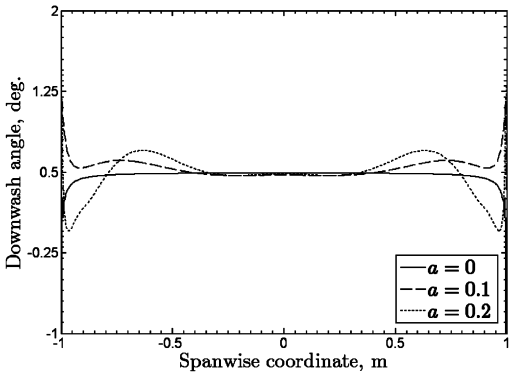

Fig. 5 Downwash angle distribution of several gull wings, $\Lambda = 10$, $\alpha = 3$ deg.

linear theory, an angle of attack of 3 deg will be used subsequently as a point for comparison.

As an example, the three wings depicted in Fig. 3 are analyzed using this lifting-line theory and compared in Figs. 4–7, using $m = M = 101$. Figure 4 shows the circulation distributions $\Gamma(y)$ for various values of curvature parameter a. As a increases, the circulation increases towards the center, where the wing behaves locally as a forward-swept wing, whereas towards the wingtips the aft sweep of the wing causes a local reduction in circulation, compared with the elliptical distribution of the straight wing case. The downwash angle $\varepsilon(y)$, computed from Eq. (39), is plotted in Fig. 5. The downwash is nearly constant in the case of the straight elliptical wing ($a = 0$), as predicted by Prandtl [13] and Munk [12]. As the wing curvature increases, downwash on the forward-swept sections of the wing increases while decreasing across the aft-swept portions. Similar effects of swept curvature on downwash angle have been shown for parabolic wings by Prössdorf and Tordella. They note that the largest decrease in induced velocity occurs towards the wingtips [7]. Figure 6 is a plot of the lift force per unit length

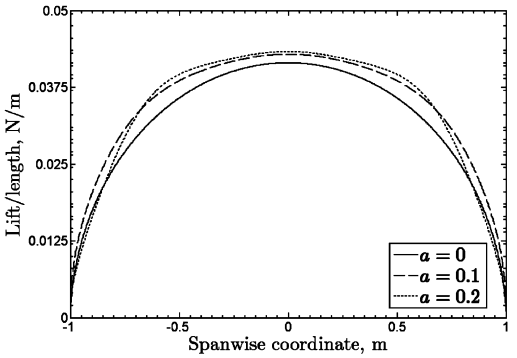

Fig. 6 Lift per unit length distribution of several gull wings, $\Lambda = 10$, $\alpha = 3$ deg.

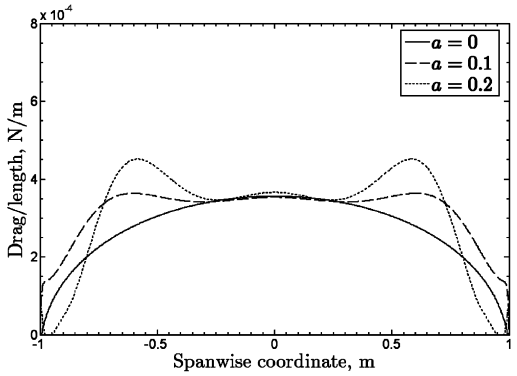

Fig. 7 Drag per unit length distribution of several gull wings, $\Lambda = 10$, $\alpha = 3$ deg.

distribution across the same three gull wings, whereas Fig. 7 displays the drag force. As expected, the lift and drag distributions are both elliptical for the straight wing case. The lift distributions are approximately equal to the circulation distributions, scaled by a factor of ρU_∞, because in all cases the downwash angles are small. Similarly, the drag distributions follow the same patterns as the downwash angle distributions. These plots indicate the gull wing's ability to shift the center of lift forward as the wing morphs from straight to curved, although a drag penalty is incurred.

The preceding comparison of several gull wings of constant span (and aspect ratio) is desired from a purely theoretical stance because aspect ratio is an important nondimensional parameter when discussing finite wings. For example, aspect ratio is a major factor in comparing the lift-to-drag ratios of several wings of similar shape. However, when developing and analyzing morphing wing designs, a constant aspect ratio is often difficult to maintain due to practical limits on planform deformation. Variable-swept wing aircraft such as the F-111 and the F-14 clearly exemplify the reduction in aspect ratio that morphing wing technologies suffer. To return to the previous example, Fig. 8 depicts several gull wings of the same curvature parameters as before but now with constant arc length. These wings more clearly illustrate the deformations caused by bending a straight wing along the quarter-chord line in order to achieve a gull-like geometry. Once again these wings are curved in such a way as to maintain a constant center of gravity location. These wings are compared with the wings depicted in Fig. 3 in Table 1 below. As expected, the wings of smaller aspect ratio have reduced lift-to-drag efficiency. This effect is much greater than merely changing the curvature of constant aspect ratio wings. Also note that there is a maximum in drag force within this range of curvature parameter for wings of constant span. Initially drag increases with curvature due to added downwash over the forward-swept sections of the wing; however, at higher curvatures this is mitigated by the reduced downwash over the highly aft-swept wingtip sections.

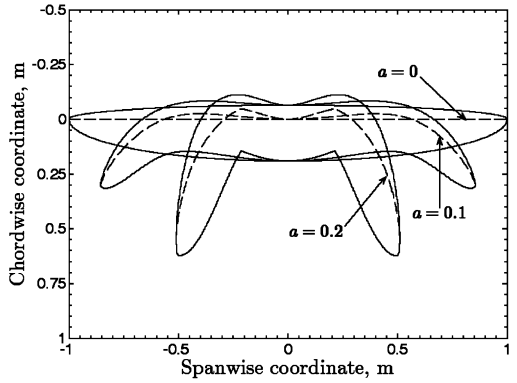

Fig. 8 Gull wings of constant arc length with curvature parameter $a = 0, 0.1, 0.2$.

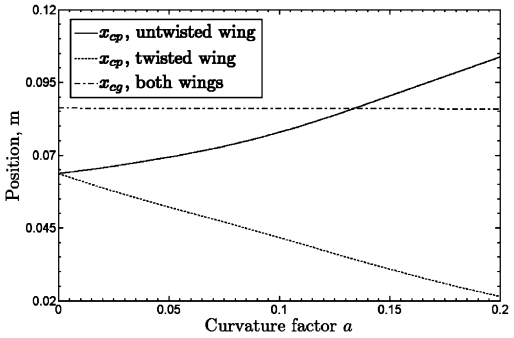

Fig. 9 Variation in c.p. and c.g. for twisted and untwisted gull wings on the interval $a = [0, 0.2]$, $\theta_{\max} = 5$ deg.

Table 1 Comparison of several gull wings

	Wings of constant span			Wings of constant arc length		
a	Lift, N	Drag, N	Lift/Drag	Lift, N	Drag, N	Lift/Drag
0	0.0645	5.436e − 4	118.6	0.0645	5.436e − 4	118.6
0.1	0.0695	6.296e − 4	110.3	0.063	7.287e − 4	86.45
0.2	0.0688	6.248e − 4	110.0	0.0417	8.999e − 4	46.31

As shown by Table 1, morphing a straight wing into a gull-like configuration is useful for lift reduction for higher speed flight. For example, a high endurance reconnaissance aircraft may morph its wings by increasing their curvature parameter a in order to perform a high-speed dive in order to evade an enemy. The added feature of forward- and aft-swept wing sections allows the manipulation of the center of pressure if wing twist can be commanded as a function of span. Figure 9 shows the variation in centers of pressure and gravity with curvature parameter for gull wings of constant wingspan. Untwisted wings, like those discussed above, are compared with twisted wings with twist distributions of the form

$$\theta(y) = \theta_{\max} \sin\left(\frac{\pi}{k}|y|\right) \tag{41}$$

where once again $k = \sqrt{3/7}$. Figure 9 indicates that with a maximum twist of only 5 deg, the center of pressure can be shifted forward by 18% of the root chord while not moving the center of gravity. Thus, a change in wing configuration from straight to gull can be used to reduce the static margin of the aircraft, for example.

Conclusion

An extension of Weissinger's method to curved wings provides a useful analysis tool for the preliminary design of morphing wings. This method can be easily applied to wings whose geometry can be described by piecewise analytical functions. The analytical nature of this technique allows specific geometrical parameters to be varied and their effects on the wing's aerodynamics to be analyzed; however, caution must be taken when considering flows where viscous effects dominate. In this paper, a morphing gull wing is analyzed in the cases of both constant span and constant arc length. It is shown that increased curvature of the wing results in reduced lift and lift-to-drag efficiency, confirming this morphology's usefulness in loiter to high-speed dash reconfiguration. Also, this wing's ability to manipulate its center of pressure location relative to its center of gravity is discussed. Each of these studies demonstrates the usefulness of this analysis technique, as long as the bounds of this method's validity are not overstepped.

Acknowledgments

This work is supported by the NASA Langley Research Center through the Graduate Student Research Program; Grant No. NGT-1-03022. The NASA technical advisors for this grant are Martin Waszak and Anna-Maria McGowan.

References

[1] Sanders, B., Crowe, R., and Garcia, E., "Defense Advanced Research Projects Agency—Smart Materials and Structures Demonstration Program Overview," *Journal of Intelligent Material Systems and Structures*, Vol. 15, 2004, pp. 227–233.

[2] Bowman, J., Sanders, B., and Weisshaar, T., "Evaluating the Impact of Morphing Technologies on Aircraft Performance," AIAA Paper 2002-1631, 2002.

[3] Wickenheiser, A., Garcia, E., and Waszak, M., "Evaluation of Bio-Inspired Morphing Concepts with Regard to Aircraft Dynamics and Performance," *Proceedings of SPIE—The International Society for Optical Engineering*, Vol. 5390, 2004, pp. 202–211.

[4] McGowan, A. R., "AVST Morphing Project Research Summaries in FY 2001," NASA TM-211769-2002, 2002.

[5] Wickenheiser, A., Garcia, E., and Waszak, M., "Longitudinal Dynamics of a Perching Aircraft Concept," *Proceedings of SPIE—The International Society for Optical Engineering*, Vol. 5764, 2005, pp. 192–202.

[6] Weissinger, J., "The Lift Distribution of Swept-Back Wings," NACA TM-1120, 1947.

[7] Prössdorf, S., and Tordella, D., "On an Extension of Prandtl's Lifting Line Theory to Curved Wings," *Impact of Computing in Science and Engineering*, Vol. 3, No. 3, 1991, pp. 192–212.

[8] Chiocchia, G., Tordella, D., and Prössdorf, S. "The Lifting Line Equation for a Curved Wing in Oscillatory Motion," *Zeitschrift fuer Angewandte Mathematik und Mechanik*, Vol. 77, No. 4, 1997, pp. 295–315.

[9] DeYoung, J., and Harper, C. W., "Theoretical Symmetric Span Loading at Subsonic Speeds for Wings Having Arbitrary Plan Form," NACA Report No. 921, 1948.

[10] Multhopp, H.. "Die Berechnung der Auftriebsverteilung von Tragflgeln (The Calculation of the Lift Distribution of Wings)," *Luftfahrt-forschung*, Vol. 15, 1938, pp. 153–169 (translated as British RTP translation No. 2392).

[11] Glauert, H., *The Elements of Aerofoil and Airscrew Theory*, The University Press, Cambridge, 1943.

[12] Munk, M. M., "The Minimum Induced Drag of Airfoils," NACA Report 121, 1921.

[13] Prandtl, L., *Essentials of Fluid Dynamics*, Hafner Publishing Company, New York, 1952, pp. 206–215.